Supplementary Material

Figures S1 to S3

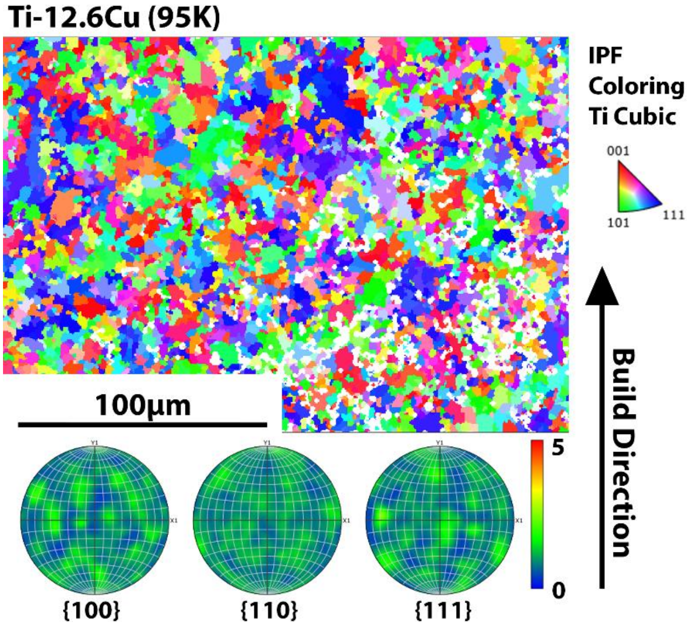

Figure S1: Parent β-grain EBSD reconstruction from the centre of the Ti-12.6Cu alloy, after undergoing thermal cycling due to the layer-by-layer manufacturing. EBSD reconstruction was generated using Aztec Crystal software. 95K references the value for *Q*. The ultra refined grains are due to the solid-solid pearlitic α/Ti_2Cu transformation during thermal cycling [1].

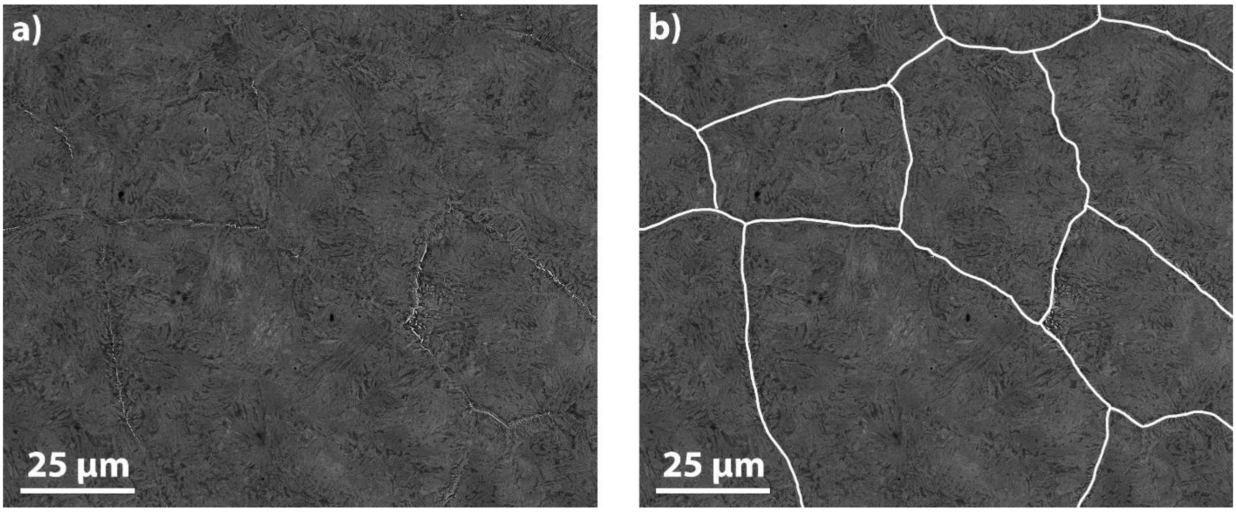

Figure S2: BSE images showing (a) The top layer of deposition of Ti-12.6Cu, showing clear prior β-grain boundaries without additional thermal cycling. (b) Outlined grains appear 50-150 µm in size.

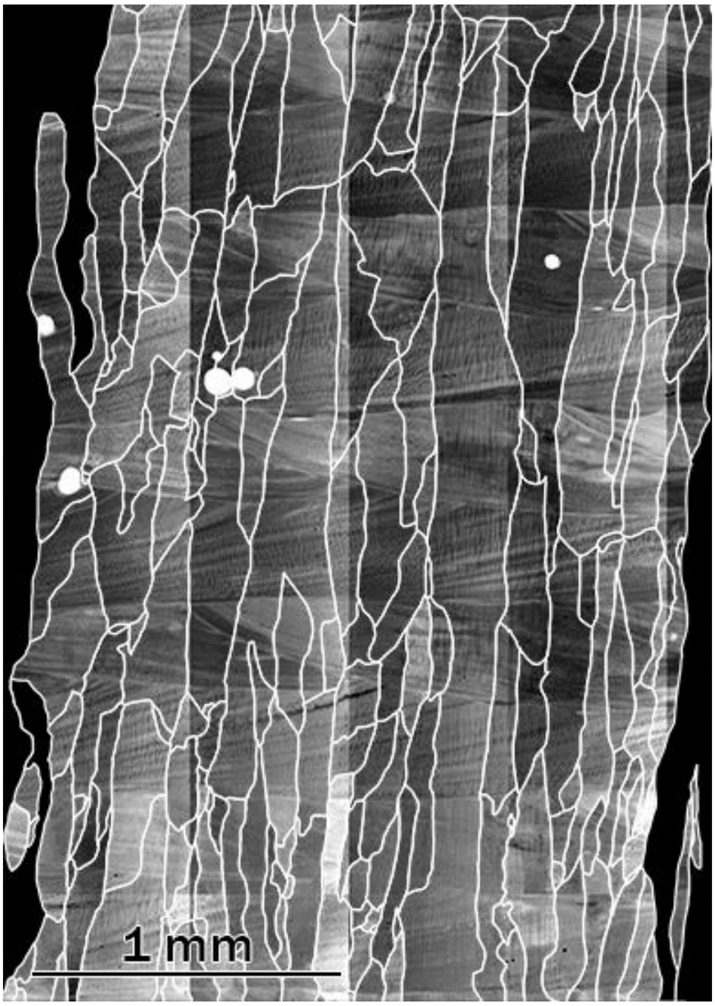

Figure S3: Ti-12Mo produced at 900W, showing large columnar grains. Grains outlined and measured using ImageJ image processing software.

Tables S1 to S8

Table S1: Produced Ti-Cu, Ti-Fe, Ti-Cu-Fe and Ti-12Mo alloys and their corresponding grain morphology, where AR is the aspect ratio. Ti-12Mo at 900W is additionally shown in Figure S3. Shading corresponds to columnar (dark grey), columnar + equiaxed (light grey) and equiaxed (white) microstructures.

Composition	ΔT_s (K)	Q (K)	P (K)	Area Weighted Mean Grain Size (µm)(± SD)	Area Weighted AR (± SD)		Grain Morphology (C- columnar; E-equiaxed)
Ti4Fe	595	42	111	186.8 ± 63.8	2.2 ± 0.7		C+E
Ti2.4Cu2.4Fe	677	42	104	200.8 ± 72.2	2.5 ± 1.3		C+E
Ti6Cu	633	43	108	258.8 ± 76.6	4.0 ± 1.2		C
Ti8Fe	532	91	176	107.1 ± 35.9	1.8 ± 0.8		E
Ti4.7Cu4.7Fe	609	89	172	132.3 ± 46.9	1.7 ± 0.8		E
Ti12.6Cu	552	95	243	65.00 ± 46.0	1.8 ± 0.8		E
Ti-12Mo	105	76	45	751.0 ± 482.0	6.0 ± 3.0		C

Table S2: Ti-xCu-yFe alloys and their corresponding ΔT_s, Q, P and grain morphology. As taken from [2]. Shading corresponds to columnar (dark grey), columnar + equiaxed (light grey) and equiaxed (white) microstructures.

Composition	ΔT_s (K)	Q (K)	P (K)	Area weighted AR (± SD)	Grain morphology (C- columnar; E-equiaxed)	Reference
Ti-6Cu-6Fe	566	117	197	1.9 ± 0.9	E	[2]
Ti-4Cu-6Fe	595	100	181	1.5 ± 0.6	E	[2]
Ti-6Cu-4Fe	604	91	177	1.6 ± 0.7	E	[2]
Ti-4Cu-4Fe	631	74	154	1.7 ± 0.8	E	[2]
Ti-2Cu-4Fe	657	58	133	2.4 ± 0.9	C+E	[2]
Ti-4Cu-2Fe	664	50	117	2.1 ± 0.6	C+E	[2]
Ti-2Cu-2Fe	688	35	89	4.5 ± 2.4	C	[2]

Table S3: Ti-6Al-4V-xNi, Ti-18, Ti-18+3Fe and their corresponding ΔT_s, Q, P and Grain morphology. As taken from [3]. Shading corresponds to columnar (dark grey), columnar + equiaxed (light grey) and equiaxed (white) microstructures.

Composition	ΔT_s (K)	Q (K)	P (K)	Grain morphology (C- columnar; E-equiaxed)	Reference
Ti-6Al-4V-3.5Ni	698	64	378	E	[3]
Ti-6Al-4V-1.7Ni	727	36	200	C+E	[3]
Ti-6Al-4V-0.5Ni	741	18	77	C	[3]
Ti-5.5Al-5V-5Mo-2.4Cr-3.75Fe-0.15O (Ti-18+3Fe)	516	81	98	C+E	[3]
Ti-5.5Al-5V-5Mo-2.4Cr-0.75Fe-0.15O (Ti-18)	278	36	51	C	[3]

Table S4: Ti-xCu alloys and their corresponding ΔT_s, Q, P and Grain morphology. As taken from [4] and [5]. Average grain size also given as taken from [5].

Composition	ΔT_s (K)	Q (K)	P (K)	Grain morphology (C-columnar; E-equiaxed)	Reference
Ti-6.8Cu	623	49	123	E	[4]
Ti-2.5Cu	672	17	45	E	[4]
Ti-8.5Cu	603	62	156	E (Average: 9.6 μm)	[5]
Ti-6.5Cu	627	46	118	E (Average: 16.3 μm)	[5]
Ti-3.5Cu	661	24	63	E (Average: 69.8 μm)	[5]

Table S5: Ordinary least square linear fit from Figure 4.

Parameter	**Linear Equation**	R^2
$\boldsymbol{\Delta T_s}$	$\mathbf{AR^{-1}} = 0.444\text{x}10^{-3} \times \boldsymbol{\Delta T_s} + 0.217$	0.203
$\boldsymbol{Q}$	$\mathbf{AR^{-1}} = 3.349\ \text{x}10^{-3} \times \boldsymbol{Q} + 0.231$	0.334
$\boldsymbol{P}$	$\mathbf{AR^{-1}} = 3.388\ \text{x}10^{-3} \times \boldsymbol{P}$	0.810

Table S6: Calculated values for numerical CET model and Rosenthal's equation.

	Ti-4Fe	**Ti-8Fe**	**Ti-12Mo**
Thermal gradient ($K.m^{-1}$) - *G*	$10.20\text{x}10^5$	$8.59\text{x}10^5$	$12.62\text{x}10^5$
Solidification velocity ($m.s^{-1}$) - *V*	$1.12\text{x}10^{-2}$	$1.13\text{x}10^{-2}$	$1.12\text{x}10^{-2}$

Table S7: Variables used in the calculation of CET models.

	Ti-4Fe	**Ti-8Fe**	**Ti-12Mo**	**Ref.**
N_0 (m^{-3}) – Nucleant density	$2\text{x}10^{12}$	$2\text{x}10^{12}$	$2\text{x}10^{12}$	-
ΔT_n (K) – Nucleation undercooling	0.75	0.75	0.75	[6]
D ($m^2 \cdot s^{-1}$) – Solute diffusion coefficient in liquid	$1.2\text{x}10^{-8}$	$1.2\text{x}10^{-8}$	$1.2\text{x}10^{-8}$	[7]
***k* – Partition coefficient**	0.36	0.36	1.67	-
***Co* (wt.%) – Nominal concentration**	4	8	12	-
Γ (K.m) – Gibbs-Thomson coefficient	$1.88\text{x}10^{-7}$	$1.88\text{x}10^{-7}$	$1.88\text{x}10^{-7}$	[8]
m_l ($K.wt.\%^{-1}$) – liquidus slope	-14.46	-14.46	9.15	-
σ^* - dendrite-tip selection parameter	0.025	0.025	0.025	[8]
***Q* (K)**	42	91	76	-
ΔT_0 (K) (*P*)	111	176	45	-

Table S8: Variables used in the calculation of the Rosenthal equation.

	Ti-4Fe	Ti-8Fe	Ti-12Mo	Ref.
Liquidus Temperature (K)	1923	1817	2046	-
τ (W.m^{-1}.K^{-1}) – Thermal conductivity	23.23	22.46	24.72	-
V_l (m.s^{-1}) – Laser scan speed	0.015	0.015	0.015	-
α (m^2.s^{-1}) – Thermal diffusivity	9.73x10^{-6}	9.33x10^{-6}	10.39x10^{-6}	-
z (m) – Melt pool depth	-2.5x10^{-4}	-2.5x10^{-4}	-2.5x10^{-4}	-
λ - Absorptivity	0.5	0.5	0.5	[9]
P (W) – Laser power	900	900	900	-

References

[1] A. I. Saville *et al.*, "Fine-grained Ti-Cu microstructures by solid state thermal cycling," *Additive Manufacturing,* vol. 75, p. 103747, 2023/08/05/ 2023, doi: https://doi.org/10.1016/j.addma.2023.103747.

[2] R. Brooke *et al.*, "Novel bainitic Ti alloys designed for additive manufacturing," *Materials & Design,* vol. 244, 2024, doi: 10.1016/j.matdes.2024.113176.

[3] B. A. Welk, N. Taylor, Z. Kloenne, K. J. Chaput, S. Fox, and H. L. Fraser, "Use of Alloying to Effect an Equiaxed Microstructure in Additive Manufacturing and Subsequent Heat Treatment of High-Strength Titanium Alloys," *Metallurgical and Materials Transactions A,* vol. 52, no. 12, pp. 5367-5380, 2021, doi: 10.1007/s11661-021-06475-3.

[4] M. Nartu *et al.*, "Underlying factors determining grain morphologies in high-strength titanium alloys processed by additive manufacturing," *Nat Commun,* vol. 14, no. 1, p. 3288, Jun 6 2023, doi: 10.1038/s41467-023-38885-9.

[5] D. Zhang *et al.*, "Additive manufacturing of ultrafine-grained high-strength titanium alloys," *Nature,* vol. 576, no. 7785, pp. 91-95, Dec 2019, doi: 10.1038/s41586-019-1783-1.

[6] J. D. Hunt, "Steady state columnar and equiaxed growth of dendrites and eutectic," *Materials Science and Engineering,* vol. 65, no. 1, pp. 75-83, 1984/07/01/ 1984, doi: https://doi.org/10.1016/0025-5416(84)90201-5.

[7] J. Kundin *et al.*, "Phase-field modeling of eutectic Ti–Fe alloy solidification," *Computational Materials Science,* vol. 63, pp. 319-328, 2012, doi: 10.1016/j.commatsci.2012.06.033.

[8] A. E. Davis *et al.*, "Achieving a Columnar-to-Equiaxed Transition Through Dendrite Twinning in High Deposition Rate Additively Manufactured Titanium Alloys," *Metallurgical and Materials Transactions A,* vol. 55, no. 6, pp. 1765-1787, 2024, doi: 10.1007/s11661-024-07388-7.

[9] P. Promoppatum, S.-C. Yao, P. C. Pistorius, and A. D. Rollett, "A Comprehensive Comparison of the Analytical and Numerical Prediction of the Thermal History and Solidification Microstructure of Inconel 718 Products Made by Laser Powder-Bed Fusion," *Engineering,* vol. 3, no. 5, pp. 685-694, 2017, doi: 10.1016/j.Eng.2017.05.023.